Revised interpretation of recent InSAR signals observed at Llaima volcano (Chile)

Dominique Rémy, Y Chen, Jean-Luc Froger, Sylvain Bonvalot, L. Cordoba, J. Fustos

AGU PUBLICATIONS

Geophysical Research Letters

RESEARCH LETTER
10.1002/2015GL063872

Key Points:
- The 2008 Llaima eruption was not accompanied by InSAR-detectable displacement
- Tropospheric delay may produce volcano-wide effect up to 2.7 fringes in C band

Supporting Information:
- Figure S1
- Figure S2
- Figure S3
- Figures S1–S3 and Table S4

Correspondence to:
D. Remy,
remy@ird.fr

Citation:
Remy, D., Y. Chen, J. L. Froger, S. Bonvalot, L. Cordoba, and J. Fustos (2015), Revised interpretation of recent InSAR signals observed at Llaima volcano (Chile), *Geophys. Res. Lett.*, *42*, 3870–3879, doi:10.1002/2015GL063872.

Received 18 MAR 2015
Accepted 1 MAY 2015
Accepted article online 7 MAY 2015
Published online 29 MAY 2015

Revised interpretation of recent InSAR signals observed at Llaima volcano (Chile)

D. Remy[1], Y. Chen[1], J. L. Froger[2], S. Bonvalot[1], L. Cordoba[3], and J. Fustos[4,5]

[1]GET/UMR5563 (UPS, CNRS, IRD, CNES), Observatoire Midi-Pyrénées, Université P. Sabatier, Toulouse, France, [2]LMV/UMR6524 (UBP-CNRS-IRD), Observatoire de Physique du Globe de Clermont-Ferrand, Université B. Pascal, Clermont-Ferrand, France, [3]SERNAGEOMIN, Observatorio Volcanológico de Los Andes del Sur, Temuco, Chile, [4]Department of Geophysics, University of Concepcion, Concepcion, Chile, [5]School of Environmental Sciences, Catholic University of Temuco, Chile

Abstract We analyzed C band and L band interferometric synthetic aperture radar (InSAR) data acquired from 2003 to 2011 to search for volcanic deformations at Llaima volcano, Southern Andes (38.69°S, 71.73°W). There, specific environmental conditions (steep slopes, snow- or ice-capped summit, dense vegetation cover, and strong tropospheric artifacts) and limited amount of radar data available make it challenging to accurately measure ground surface displacement with InSAR. To overcome these difficulties, we first performed a careful analysis of the water vapor variations using Medium-Resolution Imaging Spectrometer and Moderate Resolution Imaging Spectroradiometer near-infrared water vapor products and then we inverted wrapped interferograms for both topographic correlated phase delays and a simple model source strength. In the light of our results, we conclude that there is no detectable ground displacement related to a deep magmatic source for the 2003–2011 period and that most of the fringes observed in the interferograms were produced by tropospheric delays.

1. Introduction

Since the pioneering study on Mount Etna by *Massonnet et al.* [1995], interferometric synthetic aperture radar (InSAR) data have been widely used to monitor surface displacement related to volcanic activity in various contexts [e.g., *Massonnet and Sigmundsson*, 2000; *Dzurisin*, 2003; *Sparks*, 2003; *Pritchard and Simons*, 2004; *Fournier et al.*, 2010; *Lu and Dzurisin*, 2014; *Pinel et al.*, 2014]. However, for many active volcanoes worldwide, and particularly for explosive andesitic volcanoes, obtaining reliable displacement measurements from InSAR remains a challenge. The main reason is that most of these volcanoes are located in intertropical or temperate areas where the combination of frequent precipitations and fertile soils favors the development of dense vegetation that causes temporal decorrelation of interferometric phases [*Pinel et al.*, 2011; *Ebmeier et al.*, 2013]. Snow cover, summit ice caps, or rapid gullying of loose ground can also contribute to temporal decorrelation [*Lu and Dzurisin*, 2014]. In addition, andesitic volcanoes often have steep slopes, resulting in strong geometric distortions (foreshortening—layover) in SAR images and thus in information loss. A last difficulty arises from changes in the phase delay related to spatial and temporal variations of the physical and chemical properties of the troposphere between successive SAR acquisitions. These changes result in long- and short-wavelength artifacts in the interferograms. Various approaches have been proposed in order to mitigate these tropospheric bias in the interferograms [*Zebker et al.*, 1997; *Beauducel et al.*, 2000; *Remy et al.*, 2003; *Pavez et al.*, 2006; *Puysségur et al.*, 2007; *Doin et al.*, 2009; *Fournier et al.*, 2011; *Pinel et al.*, 2011, 2014]. However, none of them have been entirely successful, and a reliable ready-made solution does not as yet exist. In this situation, discriminating real ground surface displacement from a tropospheric signal can represent a real challenge, and interpreting the interferometric signal in terms of magmatic process requires extreme caution.

Llaima (38.69°S, 71.73°W; 3125 m) is one of the largest Andean volcanoes, with an area of 500 km^2 and a volume of 400 km^3 (Figure 1), and also one of the most active, with more than 48 known eruptions since 1640 [*Moreno et al.*, 2009]. This complex stratovolcano is built over an 8 km wide Holocene caldera by accumulation of basaltic and andesitic lava flows, andesitic and dacitic pyroclastic flows, pumice falls deposits, and lahar deposits [*Naranjo and Moreno*, 1991]. Llaima eruptions are characterized by Strombolian, Hawaiian, and infrequent sub-Plinian eruptions. At least seven eruptions of volcanic explosivity index (VEI) ≥ 3 occurred during the past 7000 years. Its recent activity has been characterized by

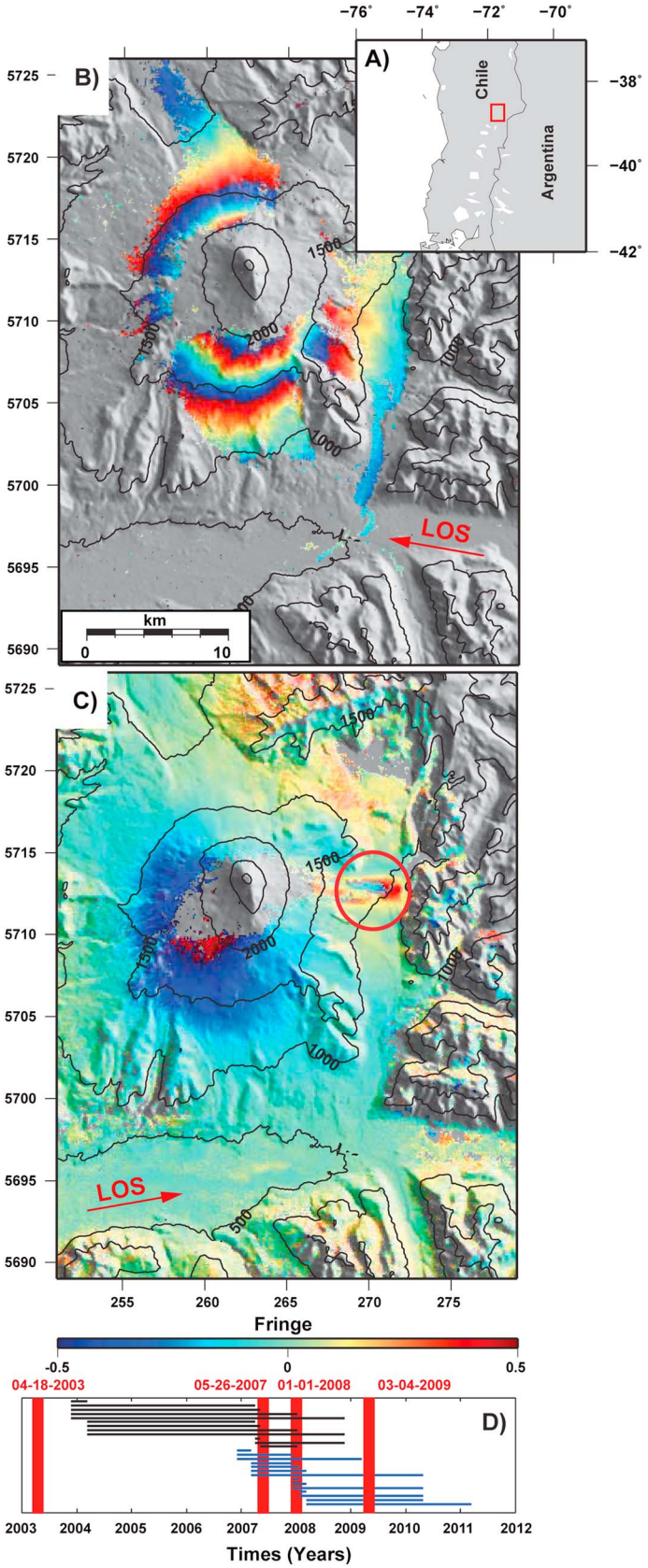
A)
B)
C)
D)
Chile
Argentina
−76°
−74°
−72°
−70°
−38°
−40°
−42°
LOS
km
0
10
Fringe
-0.5
0
0.5
04-18-2003
05-26-2007
01-01-2008
03-04-2009
Times (Years)

Figure 1

relatively small eruptions between 1979 and 2003 (11 eruptions with VEI $\leq$ 2) and by a slight increase in explosivity for the last eruptive cycle, between March 2007 and June 2009 (with 2 $\leq$ VEI $\leq$ 3) (*Smithsonian Institution Global volcanism report available at* http://www.volcano.si.edu). The largest eruption during this period of activity was on 1 January 2008, with a column reaching a height of 11 km accompanied by strong explosions and major seismic activity [*Moreno et al.*, 2009], followed by a second large eruption in 3 April 2009.

Using advanced synthetic aperture radar (ASAR) and Phased Array type L-band Synthetic Aperture Radar (PALSAR) interferograms spanning the 2002–2008 period, *Fournier et al.* [2010] failed to identify any ground displacements related to deep magmatic sources but detected a temporally complex combination of uplift and subsidence of up to 11 cm on the eastern flank of the volcano. The authors interpreted these displacements as being related to a slow landslide, in agreement with field observations. Using ASAR interferograms spanning the same period as those used by *Fournier et al.* [2010], *Bathke et al.* [2011] detected interferometric signals centered on the volcanic edifice. Contrary to what was claimed by *Fournier et al.* [2010], *Bathke et al.* [2011] interpreted these signals in terms of two main displacement episodes: a summit subsidence of ~10 cm from November 2003 to May 2007, followed by uplift of ~8 cm from May 2007 to January 2008. Through inverse modeling, the authors proposed that these volcanic deformation episodes were associated with a volume decrease of $10–46 \times 10^6\,m^3$ followed by a volume increase of $6–20 \times 10^6\,m^3$ of a magma body located beneath Llaima volcano.

In this study, we analyzed ASAR and PALSAR data acquired during several periods of volcanic activity from 2003 to 2011, with the objective to assess if ground surface displacements were indeed associated with these activity periods. As a significant proportion of the Llaima flanks' surface is covered by dense broadleaf and coniferous evergreen forest, the ASAR interferograms are generally heavily affected by phase decorrelation. As such decorrelation effects hardly complicate the unwrapping phase operation, we applied the General Inversion for Phase Technique (GIPhT) proposed by *Feigl and Thurber* [2009] to model the phase data directly without unwrapping. Moreover, given that Llaima volcano is close to the ocean, the atmospheric conditions can be extremely variable both temporally and spatially, leading to possible strong atmospheric artifacts in the interferograms. This is why we paid special attention to the detection of such possible artifacts by performing a close inspection of the Medium-Resolution Imaging Spectrometer (MERIS) and of the Moderate Resolution Imaging Spectroradiometer (MODIS/Terra) images collected over the study area. Indeed, the Level 2 data products of both spaceborne spectrometers include images of precipitable water vapor (PWV) from which it is possible estimating the tropospheric phase delay in InSAR data [*Li et al.*, 2003, 2006].

2. InSAR Observations

We analyzed six images of C band SAR data from the radar ASAR on board the European Space Agency (ESA) satellite Envisat (descending track 10, swath I2) and eight images of L band SAR data from the PALSAR radar on board the Japanese space agency (Japan Aerospace Exploration Agency (JAXA)) satellite ALOS1 (ascending track 117, mode fine beam single polarization) acquired between 2003 and 2011 over the study area (see Figure 1). Differential interferograms were generated with the DIAPASON software ©*Centre National d'Etudes Spatiales/Altamira-information*, 1996] using the two pass method described by *Massonnet and Feigl* [1998]. The orbital contribution was removed using precise orbit data from ESA Doppler Orbitography and Radio-positioning Integrated by Satellite (for ASAR interferograms) or orbit state vectors provided in the image header (for PALSAR interferograms). The topographic contribution was removed using the 3 arcsec Shuttle Radar Topographic Mission digital elevation model (DEM). PALSAR and ASAR

Figure 1. Example of ASAR and PALSAR interferograms overlain onto a shaded relief map computed for Llaima in southern Chile. (a) Reference map of the study area. (b) ASAR interferogram (25 November 2003 to 3 April 2007). (c) PALSAR interferogram (6 March 2007 to 11 March 2009). Each fringe (full color cycle) represents 2.83 cm (ASAR) or 11.81 (PALSAR) of range change between the ground and the satellite. Areas where the interferometric coherence is lost or not covered by the track ALOS 117 are shown in grey. Each fringe (full color cycle) represents 2.83 cm (ASAR) or 11.81 (PALSAR) of range change between the ground and the satellite. The black lines show elevation contours every 500 m. Coordinates are expressed in UTM-WGS84 coordinates (19 zone south). The satellite to ground radar line of sight is shown with a red arrow. (d) Time span covered by the 12 ASAR interferograms (in black) and the 14 PALSAR interferograms (in blue) used in this study. The vertical red lines show the timing of the eruptions which occurred during the 2003–2012 period.

interferograms were downsampled during processing to eight looks in azimuth and two looks in range, respectively. We obtained a set of 12 ASAR interferograms produced by data pairs characterized by an altitude of ambiguity (Ha) greater than 30 m (i.e., perpendicular baseline lower than 300 m) suitable for interferometry purpose. At the same time, 14 interferograms were generated by PALSAR pairs having an Ha greater than 40 m, corresponding to a perpendicular baseline lower than 1500 m.

Figure 1 shows a selection of two ASAR and PALSAR interferograms (the full set of interferograms used in this study is shown in Figures S1 and S2 in the supporting information). As expected, the PALSAR interferograms have a higher coherence than the ASAR one over the study area, as the L band wave of PALSAR penetrates more deeply into the vegetation cover and interacts with more stable scatterers [*Rosen et al.*, 1996]. The coherent areas on the C band interferograms are clearly less extended and correspond mainly to recent barren lava flows. On the southern half of the volcano summit, both bands of SAR data are heavily affected by phase decorrelation due to the presence of a glacier.

Most of the calculated interferograms exhibit a concentric pattern of fringes centered on the volcano, as previously observed by *Bathke et al.* [2011] (Figure 1 and Figures S1 and S2 in the supporting information). As the magnitude of the observed phase gradient is not correlated with the Ha in both ASAR and PALSAR interferograms, we concluded that this signal does not result from topography errors in the DEM. On the PALSAR interferogram shown in Figure 1c, we can also see the short-wavelength signal pattern on the eastern flank of the volcano (circled zone) previously identified by *Fournier et al.* [2010]

3. Analysis of Near-Infrared Water Vapor Products

Before making a further detailed analysis of the InSAR data, we analyzed the magnitude and the behavior of the water vapor variation over the study area using MERIS and MODIS PWV estimates [*Li et al.*, 2006, 2012; *Remy et al.*, 2011], as the troposheric delay (especially that due to water vapor) is considered as a major source of error source in InSAR [*Zebker et al.*, 1997; *Hanssen*, 2001; *Wadge et al.*, 2002; *Li et al.*, 2012]. Nevertheless, the estimation of atmospheric signal in interferograms using PWV estimates is only possible during the daytime and under cloud-free conditions. Consequently, the analysis of PWV estimates was not possible for PALSAR data as they were acquired during the night (~1 A.M. local time). Therefore, we analyzed MERIS near-IR products in reduced resolution mode (nadir pixel of about 1.04 km across track by 1.2 km along track) acquired simultaneously with the ASAR images used in this study. Where possible, we also used the independent information provided by MODIS images acquired less than an hour after the ASAR acquisitions over the study area. We computed the two-way SAR slant path delay (SPD) signal induced by atmospheric water vapor using the relation given by *Zebker et al.* [1997]:

$$\mathrm{SPD} = \frac{\mathrm{PWV}}{\Pi \cos\theta_{\mathrm{inc}}} \tag{1}$$

where the SPD and the PWV are expressed in meter and θ_{inc} is the incidence angle of the ASAR radar beam (~23°). Π is an atmospheric parameter that depends on the meteorological profile of pressure, temperature, and moisture along the radar beam path [*Bevis et al.*, 1996]. Since the variability of Π is generally more than an order of magnitude lower that of the PWV, Π may be treated, in a first approximation, as a constant with a value of about 0.15 [*Bevis et al.*, 1996]. Figure 2a shows the resulting SPD maps estimated from MERIS satellite data acquired over Llaima volcano in the same epochs than the SAR images used to form the interferogram shown in Figure 1b. The whole set of SPD maps is shown in Figure S3 in the supporting information. The two SPD maps presented in Figure 2a show contrasting amplitude and spatial features for the estimated phase delays computed over the study area. They reveal that the amplitude of the atmospheric phase delay due to variability in tropospheric water vapor concentration could be particularly strong (up to 12 cm) and variable in time. The low spatial resolution of MERIS data, with respect to ASAR data, does not reliably mitigate the tropospheric component in ASAR interferograms. Nevertheless, the MERIS-derived SPD maps provide useful indications about the structure and magnitude of phase delays related to vertically stratified water vapor in our subset of ASAR images. Figure 2a also shows the plot of SPD values estimated from MERIS (blue dots) and MODIS (red dot), data versus elevation. In both cases, the estimated SPD values vary strongly with the topography and are clearly related to topography-dependent water vapor variations. The strong dependence between the SPD and the elevation in mountainous regions is the basis for one of the traditional first order approaches used to mitigate atmospheric effects in interferograms. This approach consists of removing a

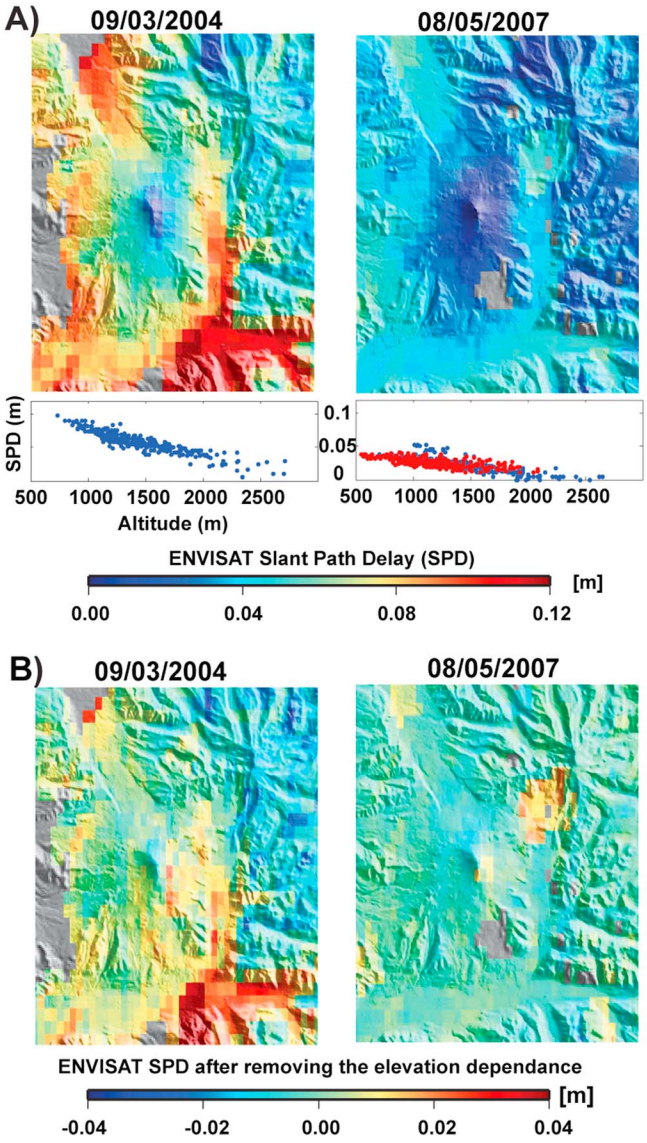

Figure 2. ASAR slant path delay estimated from MERIS satellite data acquired on 9 March 2003 and on 8 May 2007, respectively. (a) The SPD maps (top) and their respective graphs of SPD values versus elevation (bottom). The blue and red dots show values estimated from MERIS and MODIS data, respectively. Note the good agreement between the two PWV products. (b) The same fields as in Figure 2a but after removal of the elevation dependence. SPD maps are shown superimposed on the shaded-relief image, and areas that lack MERIS data are uncolored. The SPD values were interpolated using a nearest neighbor interpolation to improve the graphical quality of the figure. Note that a different color scale is used in order to better contrast the residual SPD maps.

model of SPD deduced from some linear adjustments of the dependence between elevation and the interferometric phase [*Beauducel et al.*, 2000; *Remy et al.*, 2003; *Pinel et al.*, 2011]. Figure 2b reveals that applying this approach significantly reduces the variance of the observed SPD signals in both SPD maps. Obviously, this simple elevation-dependent model is not able to capture complicated tropospheric moisture patterns. For example, the residual map derived from MERIS data acquired on 3 March 2004 reveals a spatial pattern of underprediction in the model, which extends from the summit of volcano to the southeastern valley. The reason for the presence of this pattern is unknown but it could be related to a local flow of air induced by the strong topography, as in the case of Mount Etna, Italy [*Wadge et al.*, 2002] or Soufrière Hills volcano, Montserrat [*Wadge et al.*, 2006].

According to the amplitude of the topography-dependant delay estimated from MERIS data, our analysis suggests that the set of ASAR data can be divided in two subgroups (see Figure S3 in the supporting information). The first group is composed of the images acquired on 25 November 2003, 9 March 2004, and 18 November 2008, which are characterized by strong negative delay-elevation gradients of about −0.04 m per 1000 m of elevation. On other hand, the images acquired on 3 April 2007 and 8 May 2007 are characterized by lower negative delay-elevation gradients of about −0.02 m per 1000 m of elevation. This leads us to expect that all the interferograms formed using an image belonging to the first group, and those belonging to the second group may have been contaminated by significant vertical stratification effects.

4. Modeling Strategy

Due to the large surface area affected by phase decorrelation in the Llaima region, we did not use the standard approach of unwrapping fringe maps. We chose instead to apply the GIPhT *Feigl and Thurber* [2009] method that allows for a direct comparison between displacement models and wrapped phases and provides a robust determination both of the model misfit and of the model parameter uncertainties. In the absence of constraints on the rheological properties of the crust and on the geometry of the

magma chamber, we used a simple point source model embedded in a homogeneous elastic half-space [*Mogi*, 1958]. In order to reduce the number of parameters and the trade-off between source depth and source strength, we assumed a deformation source located at a fixed position 7 km depth below the summit, consistent with the one proposed by *Bathke et al.* [2011]. We also considered the atmosphere over the study area to be approximately horizontally homogeneous, thus inducing SPD correlated to elevation, at least at the first order [*Remy et al.*, 2003, 2011]. Our previous analysis of spatial and temporal variations of water vapor distribution from MERIS and MODIS data has shown that this correlation can be modeled satisfyingly by a simple linear equation and that the tropospheric contribution to InSAR data can be reduced significantly by removing this model, although some local turbulent effects could remain. The forward model for each interferogram is then defined by two main parameters: one for the displacement source (volume change) and one for the phase-elevation gradient corresponding to atmospheric SPD. Before inverting PALSAR interferograms, we corrected them for a two-dimensional linear ramp, after masking out the region of the Llaima volcano, in order to remove the long-wavelength signals related to orbital errors. Due to the large extent of incoherent areas in the ASAR interferograms, this correction was not possible. Even though we used precise orbits that are believed to be accurately determined, our own experience and other studies showed that significant residual orbital contribution can nevertheless remain [*Froger et al.*, 2007; *Bahr and Hanssen*, 2012; *Remy et al.*, 2014]. So for the ASAR interferograms, we added two additional parameters (horizontal components of residual orbital phase gradient) to the forward model. To invert the model parameters for each interferogram, we selected a set of coherent pixels (i.e., coherency > 0.75) equally distributed in elevation for every 50 m elevation layer (100 pixels per layer). Obviously, as it is not based on continuous spatial sampling, such an approach is valid only because phase variation in the range of 50 m altitude bands is lower than 2π, as confirmed on the interferograms. The displacement vectors computed with the source point approach [*Mogi*, 1958] at the position of the coherent selected pixels were then converted into phase values by projection along the satellite line of sight and wrapped around the half wavelength. We solved the inverse problem by maximizing the following fitness function given by *Vadon and Sigmundsson* [1997] and *Beauducel et al.* [2000]:

$$R(m) = \frac{1}{n}\left|\sum_{i=1}^{n} e^{j2\pi\left(\varphi^i_{\text{obs}} - \varphi^i_{\text{calc}}(m)\right)}\right| \tag{2}$$

where φ^i_{obs} is the observed phase and $\varphi^i_{\text{calc}}(m)$ is the computed phase using a model m for a given pixel i. As this fitness function is highly nonlinear particularly because of the phase ambiguity, we used a genetic algorithm to explore the parameters space. The inversion procedure allows both the determination of the best fitted model parameters and their confidence interval for each interferogram. To determine the uncertainties of the estimated parameters we used the parametrical statistical tests proposed by *Mardia and Jupp* [2000] and implemented by *Feigl and Thurber* [2009] in GIPhT. To enhance reliability, we adjusted the model parameters using a weighted least squares method where the weights are inversely proportional to the variance estimated by the inversion procedure [*Remy et al.*, 2003]. Furthermore, this allows us to obtain a value of volume change and of vertical phase gradient for each ASAR image relative to the image acquired on 25 November 2003, and for each PALSAR image relative to the image acquired on 6 March 2007.

5. Results

Figure 3a show the data, model, and residual for the two selected ASAR and PALSAR interferograms spanning the period November 2003 to December 2007, covering the volcanic activity which started in March 2007 (see Figures S1 and S2 in the supporting information for the whole data set). Table S4 in the supporting information also presents the best fitting source characteristics and elevation-dependent path delays for each interferogram and their uncertainties obtained by the least squares adjustment. The RMS of the residual ASAR data ranges from 3 to 7 mm, while the RMS of the residual PALSAR data is about 3 times greater, ranging from 11 to 20 mm. In some residual maps spatial patterns of strong residuals are still present, indicating that the model is not a good fit for the data, due to the simplicity of the adopted tropospheric and displacement models. We think that these spatial patterns are generally related to the complexity of the atmospheric behavior in the study area. A notable exception concerns the temporally complex ground displacement pattern on the eastern flank observed in all PALSAR interferograms encompassing the eruption of January 2008 (location shown by a circle in Figure 1c and Figure S2 in the

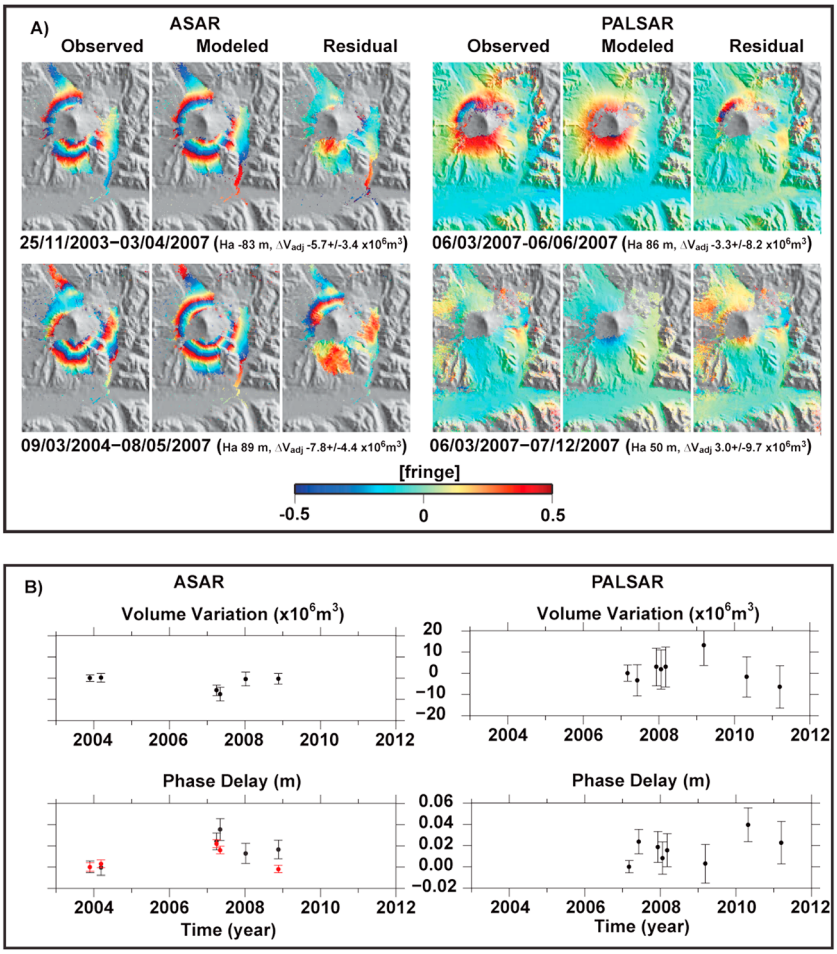

Figure 3. InSAR data and inversion results for Llaima volcano. (a) Observed, modeled, and residual between observed and modeled ground displacements. (left) ASAR interferograms scene pairs 25 November 2003 to 3 April 2007 and 9 November 2004 to 8 May 2007. (right) ALOS interferograms scene pairs 6 March 2007 to 6 June 2007 and 6 March 2007 to 7 December 2007. Each fringe (full color cycle) represents 2.83 cm (ASAR) or 11.81 (PALSAR) of range change between the ground and the satellite. The black lines show elevation contours every 500 m. Areas that lack interferometric coherence are uncolored. Interferometric phase images are shown superimposed on the shaded-relief image. In all these examples, the elevation-dependent model largely explains the observed interferometric signals. The ΔV_{adj} is the adjusted volume change and its standard deviation calculated by global L2 adjustment of the inferred values. In order to improve the quality of the figure, the interferograms were filtered using an adaptive radar interferogram filter [*Goldstein and Werner*, 1998]. (b) Estimated volume changes (ΔV) and linear contribution of tropospheric effects resulting from the adjustment with respect to the reference image acquired on 25 November 2003 for ASAR and on 6 March 2007 for PALSAR. ASAR slant path delays (SPD) estimated from MERIS data are also shown in red.

supporting information). As already mentioned, *Fournier et al.* [2010] interpreted this deformation to be related to a slow landslide triggered by the 2008 eruption.

Figure 3b shows a synthesis of the results obtained for both the ASAR and PALSAR time series, with the volume change, the elevation-related phase gradient, and their 1 sigma error bars given by the least squares adjustment. The amplitude of the inferred phase delays induced by vertically stratified water vapor in the troposphere is comparable for both the ASAR and PALSAR data sets, with a maximum absolute value of up to about 3.5 cm per 1000 m of elevation, which can produce up to 2.7 C band fringes or 0.6 L band fringes over Llaima volcano. These estimations are consistent with those obtained in the analysis carried out using the MERIS and MODIS data (section 3) and are illustrated clearly in Figure 3b by the good agreement between the ASAR slant path delays estimated from the MERIS data (in red) and those obtained from the inversion of ASAR data. This maximum phase delay of 3.5 cm per 1000 m of

elevation is large, although not exceptional, and such large effects have been documented on various sites: Mount Cameroun [*Heleno et al.*, 2010]; Sakurajima, Japan [*Remy et al.*, 2003]; Soufrière Hills [*Wadge et al.*, 2006], and Colima, Mexico [*Pinel et al.*, 2011]. From these results, we would urge caution in the interpretation of transient ground displacement lower that ±7 cm on the scale of the whole volcanic edifice, when observed in a single interferogram.

The volume changes inferred by the inversion of interferograms for the volume change are generally small and range from -7.7 to $13 \times 10^6\,m^3$ during the 2003–2011 period. The uncertainties (1σ) of the adjusted volume changes inferred by the ASAR and PALSAR data are on average about $\pm 3\,10^6\,m^3$ and $\pm 9\,10^6\,m^3$, respectively. The difference in uncertainty in the parameter estimation using L band and C band data is explained by the difference in range precision between both bands [*Sandwell et al.*, 2008]. None of the PALSAR interferograms spanning the December 2006 to March 2011 period shows signals related to a volume change within a deformation source. Through inverse modeling using ASAR data, we estimated that a magma inflation source located at 7 km depth below the summit may be subjected to a volume decrease of 0.7 to $11 \times 10^6\,m^3$, at a confidence level of 95%, between November 2003 and May 2007. However, due to the limitation of InSAR for surface change detection related to the magnitude of atmospheric perturbations in the Llaima area, as highlighted in this study, the low-volume change inferred by the inversion of SAR data must be interpreted with caution. Furthermore, it is also noteworthy that all the ASAR interferograms, which show a strong interferometric signal, are produced using ASAR images for which the difference of the phase-elevation gradients estimated from MERIS data is significant. This leads us to consider that there is no clear evidence of ground surface displacement caught by InSAR data for the 2003–2011 period and that most of the fringes observed in the interferograms of Llaima volcano are due to tropospheric effects rather than to ground surface displacements.

Different explanations could be invoked for the lack of ground displacement observed by InSAR during eruptive activity at Llaima volcano, including displacement with amplitude below the accuracy of the sensors, related to a deep source, or displacement with extension limited to the incoherent upper part of the edifice, related to a very shallow source such as a magma plug in the upper part of a conduit, or short-lived preeruptive inflation compensated by coeruptive or posteruptive deflation in a single orbital cycle [*Lu and Dzurisin*, 2014].

6. Conclusion

This study demonstrates that the applications of InSAR for detecting transient deformation induced by the activity of andesitic stratovolcanoes remain a challenge. In the Llaima area, the sparsity of the InSAR samples, the reduced surface of the coherent area, and the transient nature of the displacement expected prevented us from using stacking or Small Baseline Subset techniques [*Berardino et al.*, 2003; *Hooper*, 2008], which would make it possible to reduce and enhance the signal-to-noise ratio of the interferometric signal. This led us to carefully analyze the MERIS and MODIS water vapor products in order to assess variable phase delay through the troposphere, which can induce significant uncertainties (in the order of centimeters) in the measured displacements for a single image. This also led us to use the statistical approach proposed by *Feigl and Thurber* [2009] for analyzing wrapped phase data.

Our study does not reveal any detectable ground displacement related to a deep magmatic source under Llaima volcano in interferograms spanning the 2008 period of eruptive activity. It is worth noting that our interpretation strongly differs from that of *Bathke et al.* [2011], who considered the atmospheric effects as being negligible in their study. Our results strengthen those of *Fournier et al.* [2010] because they are now supported by a rigorous analysis of tropospheric phase delay effects related to water vapor variations in SAR interferograms.

Future geodetic studies from InSAR data on Llaima will benefit greatly from the first continuous GPS network on this volcano, set up in 2012 by the Southern Andean Volcano Observatory (Observatorio Volcanológico de Los Andes del Sur). Ground surface displacement and tropospheric delays estimated by InSAR could then be compared with independent measurements provided by the permanent GPS network, significantly improving the potential to monitor volcanic events on Llaima volcano using InSAR.

Acknowledgments
ASAR data were provided by the European Space Agency (ESA) through the project Envisat-AO#857 and Category 1 #2899. PALSAR data from the ALOS satellite mission operated by the Japanese Aerospace Exploration Agency (JAXA) were used under the terms and conditions of the fourth ALOS 2 Research Announcement (project #1142). This work was supported by the Institut de Recherche pour le Développement and the Centre National d'Etudes Spatiales (CNES). Some of the figures in this paper were made using Generic Mapping Tools [*Wessel and Smith*, 1991]. Many thanks to M. Pritchard for his useful reviews, comments, and very constructive remarks that greatly improve this paper.

The Editor thanks Matthew Pritchard and an anonymous reviewer for their assistance in evaluating this paper.

References

Bahr, H., and R. Hanssen (2012), Reliable estimation of orbit errors in spaceborne SAR interferometry, *J. Geod.*, *86*(12), 1147–1164.
Bathke, H., M. Shirzaei, and T. R. Walter (2011), Inflation and deflation at the steep-sided Llaima stratovolcano (Chile) detected by using InSAR, *Geophys. Res. Lett.*, *38*, L10304, doi:10.1029/2011GL047168.
Beauducel, F., P. Briole, and J. L. Froger (2000), Volcano wide fringes in ERS synthetic aperture radar interferograms of Etna (1992–1999): Deformation or tropospheric effect?, *J. Geophys. Res.*, *105*, 16,391–16,402, doi:10.1029/2000JB900095.
Berardino, P., M. Costantini, G. Franceschetti, A. Iodice, L. Pietranera, and V. Rizzo (2003), Use of differential SAR interferometry in monitoring and modelling large slope instability at Maratea(Basilicata, Italy), *Eng. Geol.*, *68*, 31–51.
Bevis, M., S. Chiswell, S. Businger, T. A. Herring, and Y. Bock (1996), Estimating wet delay using numerical weather analysis and predictions, *Radio Sci.*, *31*, 447–487, doi:10.1029/96RS00008.
©CNES/Altamira-information (1996), Philosophie et mode d'emploi de la chaîne logicielle interférométrique DIAPASON, Toulouse, France.
Doin, M.-P., C. Lasserre, G. Peltzer, O. Cavalié, and C. Doubre (2009), Corrections of stratified tropospheric delays in SAR interferometry: Validation with global atmospheric models, *J. Appl. Geophys.*, *69*(1), 35–50.
Dzurisin, D. (2003), A comprehensive approach to monitoring volcano deformation as a window on the eruption cycle, *Rev. Geophys.*, *41*(1), 1001, doi:10.1029/2001RG000107.
Ebmeier, S. K., J. Biggs, T. A. Mather, and F. Amelung (2013), Applicability of InSAR to tropical volcanoes: Insights from Central America, *Geol. Soc. London Spec. Publ.*, *380*, 15–37.
Feigl, K., and H. Thurber (2009), A method for modelling radar interferograms without phase unwrapping: Application to the *M* 5 Fawnskin, California earthquake of 1992 December 4, *Geophys. J. Int.*, *176*(2), 491–504.
Fournier, T. J., M. E. Pritchard, and S. N. Riddick (2010), Duration, magnitude, and frequency of subaerial volcano deformation events: New results from Latin America using InSAR and a global synthesis, *Geochem. Geophys. Geosyst.*, *11*, Q01003, doi:10.1029/2009GC002558.
Fournier, T. J., M. E. Pritchard, and N. Finnegan (2011), Accounting for atmospheric delays in InSAR data in a search for long-wavelength deformation in South America, *IEEE Trans. Geosci. Remote Sens.*, *49*(10), 3856–3867.
Froger, J. L., D. Remy, S. Bonvalot, and D. Legrand (2007), Two scales of inflation at Lastarria-Cordon del Azufre volcanic complex, central Andes, revealed from ASAR-ENVISAT interferometric data, *Earth Planet. Sci. Lett.*, doi:10.1016/j.epsl.2006.12.012.
Goldstein, R. M., and C. L. Werner (1998), Radar interferogram filtering for geophysical applications, *Geophys. Res. Lett.*, *25*, 4035–4038, doi:10.1029/1998GL900033.
Hanssen, R. (2001), *Radar Interferometry Data Interpretation and Errors Analysis*, 308 pp., Kluwer Acad., Dordrecht, Netherlands.
Heleno, S. I. N., C. Frischknecht, N. d'Oreye, J. N. P. Lima, B. Faria, R. Wall, and F. Kervyn (2010), Seasonal tropospheric influence on SAR interferograms near the ITCZ—The case of Fogo Volcano and Mount Cameroon, *J. Afr. Earth Sci.*, *58*(5), 833–856.
Hooper, A. (2008), A multi-temporal InSAR method incorporating both persistent scatterer and small baseline approaches, *Geophys. Res. Lett.*, *35*, L16302, doi:10.1029/2008GL034654.
Li, Z., J. P. Muller, and P. Cross (2003), Comparison of precipitable water vapor derived from radiosonde, GPS and Moderate-Resolution Imaging Spectroradiometer measurements, *J. Geophys. Res.*, *108*(D20), 4651, doi:10.1029/2003JD003372.
Li, Z., E. Fielding, P. Cross, and J.-P. Muller (2006), Interferometric synthetic aperture radar atmospheric correction: Medium Resolution Imaging Spectrometer and advanced synthetic aperture radar integration, *Geophys. Res. Lett.*, *33*, L06816, doi:10.1029/2005GL025299.
Li, Z., P. Pasquali, A. Cantone, A. Singleton, G. Funning, and D. Forrest (2012), MERIS atmospheric water vapor correction model for wide swath interferometric synthetic aperture radar, *IEEE Geosci. Remote Sens. Lett.*, *9*(2), 257–261.
Lu, Z., and D. Dzurisin (2014), *InSAR Imaging of Aleutian Volcanoes: Monitoring a Volcanic Arc From Space*, *Springer Praxis Books, Geophys. Sci.*, 388 pp., Springer, New York.
Mardia, K. V., and P. E. Jupp (2000), *Directional Statistics*, 429 pp., Wiley, New York.
Massonnet, D., and K. L. Feigl (1998), Radar interferometry and its application to changes in the Earth's surface, *Rev. Geophys.*, *36*, 441–500, doi:10.1029/97RG03139.
Massonnet, D., and F. Sigmundsson (2000), Remote sensing of volcano deformation by radar interferometry from various satellites, in *Remote Sensing of Active Volcanism*, *Geophys. Monogr.*, edited by P. Mouginis-Mark, J. A. Crisp, and J. H. Fink, pp. 207–221, AGU, Washington, D. C.
Massonnet, D., P. Briole, and A. Arnaud (1995), Deflation of Mount Etna monitored by spaceborne radar interferometry, *Nature*, *375*, 567–570.
Mogi, K. (1958), Relations between the eruptions of various volcanoes and the deformation of the ground surface around them, *Bull. Earthquake Res. Inst., Univ. Tokyo* , *36*, 99–134.
Moreno, H., J. A. Naranjo, P. Pena, J. Munoz, D. Basualto, D. Delgado, C. Gallegos, C. Dungan, and C. Bouvet de Maisonneuve (2009), El ciclo eruptivo 2007–2009 del volcan Llaima, Andes del sur, paper presented at XII Congresso geologico Chileno, Santiago, 22–26 Nov.
Naranjo, J. A., and H. Moreno (1991), Actividad explosiva postglacial en el Volcán Llaima, Andes del Sur (38°45'S), *Rev. Geol. Chile*, *18*(1), 69–80.
Pavez, A., D. Remy, S. Bonvalot, M. Diament, G. Gabalda, J. L. Froger, P. Julien, D. Legrand, and D. Moisset (2006), Insight into ground deformation at Lascar volcano (Chile) from SAR interferometry, photogrammetry and GPS data: Implication on volcano dynamics and future space monitoring, *Remote Sens. Environ.*, *100*, 307–320.
Pinel, V., A. Hooper, S. De la Cruz-Reyna, G. Reyes-Davila, M. P. Doin, and P. Bascou (2011), The challenging retrieval of the displacement field from InSAR data for andesitic stratovolcanoes: Case study of Popocatepetl and Colima Volcano, Mexico, *J. Volcanol. Geotherm. Res.*, *200*(1–2), 49–61.
Pinel, V., M. Poland, and A. Hooper (2014), Volcanology: Lessons learned from synthetic aperture radar imagery, *J. Volcanol. Geotherm. Res.*, doi:10.1016/j.jvolgeores.2014.10.010.
Pritchard, M. E., and M. Simons (2004), An InSAR-based survey of volcanic deformation in the central Andes, *Geochem. Geophys. Geosyst.*, *5*, Q02002, doi:10.1029/2003GC000610.
Puysségur, B., R. Michel, and J. P. Avouac (2007), Tropospheric phase delay in interferometric synthetic aperture radar estimated from meteorological model and multispectral imagery, *J. Geophys. Res.*, *112*, B05419, doi:10.1029/2006JB004352.
Remy, D., S. Bonvalot, P. Briole, and M. Murakami (2003), Accurate measurement of tropospheric effects in volcanic area from SAR interferometry data: Application to Sakurajima volcano (Japan), *Earth Planet. Sci. Lett.*, *213*(3–4), 299–310.
Remy, D., M. Falvey, S. Bonvalot, M. Chlieh, G. Gabalda, J. L. Froger, and D. Legrand (2011), Variability of atmospheric precipitable water in northern Chile: Impacts on interpretation of InSAR data for earthquake modeling, *J. South Am. Earth Sci.*, *31*(2–3), 214–226.
Remy, D., J. L. Froger, H. Perfettini, S. Bonvalot, G. Gabalda, F. Albino, V. Cayol, D. Legrand, and M. D. Saint Blanquat (2014), Persistent uplift of the Lazufre volcanic complex (central Andes): New insights from PCAIM inversion of InSAR time series and GPS data, *Geochem. Geophys. Geosyst.*, *15*, 3591–3611, doi:10.1002/2014GC005370.

Rosen, P., S. Hensley, H. Zebker, F. H. Webb, and E. J. Fielding (1996), Surface deformation and coherence measurements of Kilauea volcano, Hawaii, from SIR-C radar interferometry, *J. Geophys. Res.*, *101*, 23,109–23,125, doi:10.1029/96JE01459.

Sandwell, D. T., D. Myer, R. Mellors, M. Shimada, B. Brooks, and J. Foster (2008), Accuracy and resolution of ALOS interferometry: Vector deformation maps of the Father's Day intrusion at Kilauea, *IEEE Trans. Geosci. Remote Sens.*, *46*(11), 3524–3534.

Sparks, R. S. J. (2003), Forecasting volcanic eruptions, *Earth Planet. Sci. Lett.*, *210*, 1–15.

Vadon, H., and F. Sigmundsson (1997), Crustal deformation from 1992 to 1995 at the Mid-Atlanctic Ridge, southwest Iceland mapped by satellite radar interferometry, *Science*, *275*, 193–197.

Wadge, G., G. S. Mattioli, and R. A. Herd (2006), Ground deformation at Soufriere Hills Volcano, Montserrat during 1998–2000 measured by radar interferometry and GPS, *J. Volcanol. Geotherm. Res.*, *152*(1–2), 157–173.

Wadge, G., et al. (2002), Atmospheric models, GPS and InSAR measurements of the tropospheric water vapour field over Mount Etna, *Geophys. Res. Lett.*, *29*(19), 1905, doi:10.1029/2002GL015159.

Wessel, P., and W. H. F. Smith (1991), Free software help map and display data, *Eos Trans. AGU*, *72*(41), 441–446, doi:10.1029/90EO00319.

Zebker, H. A., P. A. Rosen, and S. Heinsley (1997), Atmospheric effects in interferometric synthetic aperture radar surface deformation and topographic maps, *J. Geophys. Res.*, *102*, 7547–7563, doi:10.1029/96JB03804.